Respective contribution of Appl to mushroom body axon growth and long-term memory in Drosophila

Claire Marquilly, Ana Boulanger, Germain Busto, Laure Pasquer, Robert Zinzen, Bassem A. Hassan, Lee G Fradkin, Thomas Preat, Jean-maurice Dura

Respective contribution of Appl to mushroom body axon growth and long-term memory in *Drosophila*

Claire Marquilly[1], Ana Boulanger[1], Germain U. Busto[1#], Laure Pasquer[2], Robert P Zinzen[3], Bassem A Hassan[4], Lee G Fradkin[5], Thomas Preat[2] and Jean-Maurice Dura[1]

[1] IGH, Univ Montpellier, CNRS, Montpellier, France
[2] Energy & Memory, Brain Plasticity Unit, ESPCI Paris, PSL Research University, Paris, France
[3] Systems Biology Imaging Platform, Max Delbrueck Centrum in der Helmholtz Gemeinschaft, Berlin Institute for Medical Systems Biology, Berlin, Germany
[4] Institut du Cerveau-Paris Brain Institute (ICM), Sorbonne Université, Inserm, CNRS, Hôpital Pitié-Salpêtrière, Paris, France
[5] Department of Bioengineering, Stanford University, Stanford, CA USA

[#]Present address: INM, Univ Montpellier, INSERM, Montpellier, France

Summary

The Amyloid Precursor Protein (APP) is linked to Alzheimer's disease. *Appl* is the single *Drosophila* APP ortholog and is expressed in all neurons throughout development. Appl was previously shown to modulate, cell-autonomously, axon outgrowth in the mushroom bodies (MBs), the fly olfactory memory center. Furthermore, *Appl* knockdown in the MBs results in loss of memory following the association of odorants with electric shocks. Nevertheless, the memory defects of flies devoid of Appl remains unknown because $Appl^{d}$ flies, carrying the only known null allele, show an abnormal response to electric shock. We found that $Appl^{d}$ affects the normal function of *vnd*, the gene just proximal to *Appl*. We report here that *vnd* is required for MB β-branch axon outgrowth. Moreover, *vnd* is expressed in neurons close to, but not within, the MB during development and is required non-cell-autonomously for MB axon outgrowth. To decipher developmental and memory defects specifically due to a loss of only *Appl* function, we generated a precise *Appl* null allele ($Appl^{C2.1}$) by CRISPR/Cas9 genomic engineering. With $Appl^{C2.1}$, we confirmed the partial requirement for *Appl* in MB axon outgrowth but found no defects of electric shock avoidance, allowing us to test for potential memory defects. $Appl^{C2.1}$ flies showed a complete loss of long-term memory which was fully rescued by MB-restricted expression of $Appl^{+}$ only during the adult stage. Therefore, we demonstrate that the complete lack of Appl affects memory independently from structural developmental defects.

Introduction

Alzheimer's disease (AD) is associated with extracellular accumulation of amyloid fibrils derived from the Amyloid Precursor Protein (APP). APPs have therefore been intensely investigated, however their physiological function in the brain remains unclear and controversial [1-3]. Although there are three paralogues in mammals (APP, APLP1 and APLP2), *Drosophila* encodes a

single APP homologue, called *Appl*, that is expressed in all neurons throughout development. It has been shown that the type I transmembrane protein coding gene *Appl* is a conserved neuronal modulator of a Wnt planar cell polarity (Wnt/PCP) pathway, a regulator of cellular orientation within the plane of an epithelium [4]. It has been proposed that Appl is part of the membrane complex formed by the core PCP receptors Fz (*frizzled*) and Vang (*Van Gogh*) [4, 5].

The mushroom bodies (MBs) are two bilaterally symmetric structures in the central brain that are required for learning and memory [6]. Each MB is comprised of 2000 neurons that arise from 4 neuroblasts. Three types of neurons appear sequentially during development: the embryonic/early larval γ, the larval α'β', and the late larval/pupal αβ type. Each αβ neuron projects an axon that branches to send an α branch dorsally, which contributes to the formation of the α lobe, and a β branch medially, which contributes to the formation of the β lobe [7]. So far, $Appl^{d}$ is the only reported null *Appl* allele and it results from a synthetic genomic deletion removing the *Appl* locus [8]. The $Appl^{d}$-bearing chromosome was selected, after γ irradiation, as a translocation of a partial duplication of the X chromosome on the Y chromosome to a X chromosome terminal deficiency (S1 Fig). $Appl^{d}$ flies are viable, fertile and display no gross structural defects in the brain [8]. However, the *Appl* signaling pathway is required for proper axon outgrowth in the MBs since $Appl^{d}$ flies display modestly-penetrant axonal defects in αβ neurons. In particular, Appl is required cell-autonomously for β-branch axon outgrowth [4, 9]. Using *in vivo* inducible RNA interference strategies, it was shown that Appl knockdown in the MBs results in loss of memory following the association of odorants with electric shocks [10]. Nevertheless, the memory defect of *Appl* null flies cannot be assessed for aversive memory because $Appl^{d}$ flies, unlike wild-type flies, show an abnormal response to electric shock [8].

The *ventral nervous system defective* (*vnd*) gene, which is immediately proximal to *Appl*, encodes a Nk2-class homeodomain transcription factor, that acts in a context-dependent manner as an activator or repressor and is essential for the development of the nervous system. The *vnd* gene encodes two proteins: Vnd-A and Vnd-B whose mRNAs arise from two different promoters. These two proteins differ in their aminoterminal domains and are identical in the remainder of their sequences. While Vnd-A is a transcription repressor from promoters containing Nk-2 binding sites, Vnd-B directly activates transcription [11]. Flies bearing a null allele of *vnd* in hemi- or homozygous condition are embryonic lethal [12].

Interestingly, we found that the $Appl^{d}$ chromosome also genetically affects *vnd* function. To genetically dissect *Appl* and *vnd* functions, we generated CRISPR alleles that precisely deletes the *Appl* gene without affecting *vnd* function ($Appl^{C2.1}$) and that precisely deletes each one of the two *vnd* transcripts without affecting *Appl* ($vnd^{C\Delta A}$ and $vnd^{C\Delta B}$). We showed here that *vnd-A,* but not *vnd-B,* is also required for MB β-branch axon outgrowth. Unexpectedly, *vnd* is expressed in neurons close to, but not within, the MB during development and is required non-cell-autonomously, likely by promoting the production of one (or several) secreted factor(s) involved in the MB axon outgrowth. To analyze the exact developmental and memory defects due to the specific loss of the *Appl* function only, we used $Appl^{C2.1}$ and first confirmed the partial requirement of *Appl* in MB β-branch axon outgrowth. Interestingly, $Appl^{C2.1}$ flies, in contrast to $Appl^{d}$ flies, showed a normal response to electric shock but a complete loss of long term memory independently from potential defects during brain development.

Results

Generating new *Appl* CRISPR alleles

The complex chromosome structure associated with $Appl^{d}$ complicates its subsequent genetic manipulation (S1 Fig). Therefore, we intended to produce new null *Appl* alleles by removing the entire *Appl* transcriptional unit via CRISPR/Cas9-mediated deletion [13]. We recovered $Appl^{C1.4}$ and $Appl^{C2.1}$, two CRISPR *Appl* null alleles (Fig 1 and S2 Fig), following an adaptation of a published protocol in order to produce circa 50kb deletions [14]. $Appl^{d}$ MBs display a modestly-penetrant cell-autonomous axon growth defect of the β-branches which manifests as an absence of the β lobe [4, 5]. Surprisingly, we found a strong difference in the penetrance of the absence of the β lobe phenotype in the two *Appl* CRISPR alleles. Although 9% of $Appl^{C2.1}$ MBs lacked the β lobe , slightly lower than the 14.5% described for $Appl^{d}$ [15], $Appl^{C1.4}$ MBs displayed a much higher penetrance (66%) of this phenotype (Fig 1). We determined the precise deletions present in the two alleles via sequencing and found that while the $Appl^{C2.1}$ deletion precisely removed the *Appl* transcriptional unit, the $Appl^{C1.4}$ allele also removed a part of the *vnd* transcriptional unit (Fig 1). We then similarly mapped the $Appl^{d}$ deletion and found that, unlike $Appl^{C2.1}$, it removes most of the intergenic region between *Appl* and *vnd* which may influence *vnd* function (Fig 1). We then assessed, by genetic complementation tests, if the different *Appl* null alleles possibly affected *vnd* function. We used vnd^{A} a molecularly-characterized lethal allele which impacts both *vnd-B* and *vnd-A* transcripts (Fig 2) [16]. Although $Appl^{C2.1}/vnd^{A}$ MBs displayed no anatomical MB phenotypes, $Appl^{d}/vnd^{A}$ and $Appl^{C1.4}/vnd^{A}$ MBs displayed 14% and 69% of β lobe absence, respectively (Fig 2). Flies heterozygous for any of the four mutations displayed no MB phenotypes: vnd^{A}/+ (n = 72), $Appl^{C1.4}$/+ (n = 60), $Appl^{C2.1}$/+ (n = 42) and $Appl^{d}$/+ previously described [4]. Therefore, $Appl^{d}$ and $Appl^{C1.4}$ but not $Appl^{C2.1}$ affect *vnd* functions in MB development. Taken together, these data strongly suggest that *vnd*, the gene just proximal to *Appl*, is also involved in the MB β-branch axon growth and likely to a much greater extent than *Appl* itself.

Generation of new *vnd* CRISPR alleles deleted either for the *vnd-B* or for the *vnd-A* function

There are two *vnd* transcripts, *vnd-A* and *vnd-B* that produce two different Vnd proteins, respectively Vnd-A and Vnd-B (Fig 2). It was proposed that, while Vnd-A has a main role during embryogenesis, Vnd-B is associated with metamorphosis [11]. In order to determine which Vnd isoform is required for MB β-branch axon growth, we produced the new *vnd* alleles $vnd^{C\Delta A}$ and $vnd^{C\Delta B}$ by CRISPR/Cas9 genomic engineering that eliminate either the *vnd-A* or the *vnd-B* isoform, respectively (Fig 3 and S3 Fig). Males bearing a $vnd^{C\Delta B}$ mutant allele ($vnd^{C\Delta B}$/Y), as well as $vnd^{C\Delta B}/Appl^{C1.4}$ females, are viable and have essentially wild-type MBs (Fig 3). Males bearing a $vnd^{C\Delta A}$ mutant allele ($vnd^{C\Delta A}$/Y) are embryonic lethal similarly to other *vnd* null alleles (vnd^{A}, $vnd^{\Delta 38}$ and vnd^{6}) which affect both isoforms. Also, $Appl^{C1.4}/vnd^{C\Delta A}$ female MBs displayed a strong phenotype of β lobe absence with a penetrance (64%) similar to those of $Appl^{C1.4}/vnd^{A}$ female MBs (Fig 4). Genetically, $Appl^{C1.4}/vnd^{C\Delta A}$; $Dp\text{-}Appl^{+}$/+ females have two wild-type doses of $Appl^{+}$ and the β lobe absence phenotype (69%) was not distinguishable from that observed in $Appl^{C1.4}/vnd^{C\Delta A}$; +/+ females (64%) and therefore be entirely due to *vnd* lack-of-function. Supporting this hypothesis, we observed a complete rescue when an extra dose of vnd^{+} is supplied in $Appl^{C1.4}/vnd^{C\Delta A}$; $Dp\text{-}vnd^{+}$/+ females (Fig 4). $Appl^{C1.4}$/Y males have no $Appl^{+}$ function (null allele) and also display reduced vnd^{+} function. Moreover, $Appl^{C1.4}$/Y male MB phenotype is moderately rescued by the presence of an extra dose of $Appl^{+}$ and strongly rescued by an extra dose of vnd^{+} (Fig 4). Taken

together, these results strongly indicate that the *vnd-A* transcript but not the *vnd-B* transcript is specifically required for MB β-branch axon growth.

Vnd is expressed around the MBs and is not required within the MBs

In order to know where *vnd* is expressed, we employed a *vnd-T2A-GAL4* line where GAL4 is under the control of endogenous *vnd* regulatory sequences via CRISPR gene targeting so that GAL4 and *vnd* are translated from the same mRNA transcript [17, 18]. UAS-GFP labelling revealed a pattern in the ventral ganglion of the third larval instar central nervous system (L3 CNS) similar to that described with immunostaining with antibodies against Vnd [11] thus validating the use of the *vnd-T2A-GAL4* line as a *bona fide vnd* reporter (S4 Fig). GFP was detected, in the developing brain, close to the MBs visualized by anti-Fas2 staining, from L3 to 24 h after puparium formation (APF) (Fig 5A,A'- 5D,D'). Staining reveals two different morphological structures: one organized in a honeycomb pattern and one containing filamentous structures with neurite appearance. To determine the identity of the honeycomb structures, we performed DAPI staining at the L3 stage. We observed a significant DAPI staining in these structures indicating that they likely correspond to cell nuclei (Fig 5EE'). Moreover, these cell nuclei are Vnd positive and Repo negative (Fig 5F,F'-5G,G') indicating that these cells correspond to neurons, rather than glia. The neurites corresponding to these cell nuclei are very close to the developing MB medial lobe from which the adult β lobe develops (Fig 5). Noticeably, we could not observe any GFP labeling within the MBs themselves. This unexpected expression pattern suggests a non-cell-autonomous role for Vnd in the MB β-branch axon growth. We tested this hypothesis by MARCM mosaic analysis which allows the generation of homozygous *vnd* loss-of-function MB clones in an otherwise heterozygous genetic background and overcome organismal lethality [7, 19]. Mitotic recombination was induced in late-stage embryos/early first instar larvae and the clones were analyzed at the adult stage. We obtained 20 MB $vnd^{A/A}$ clones that include the αβ neurons. All the 20 *vnd* mutant clones displayed a β-branch axon growth that looked identical to that in wild-type clones (S5 Fig). Moreover, we obtained similar results, namely a normal β-branch axon growth, with two additional different null alleles, $vnd^{\Delta 38}$ (8 clones) and vnd^{6} (4 clones) (S5 Fig). Taken together, these results demonstrate that, although *vnd* function is strongly required for MB β-branch axon growth, *vnd* is neither required nor expressed in the MBs themselves. Therefore, it is most likely that Vnd regulates MB axon growth by a non-cell-autonomous mechanism.

***Appl*-null flies have no long-term memory strictly due to the absence of Appl in adult MBs**

Although it is clear that *Appl* function is required for aversive olfactory memory, it has not yet been possible to assess the memory of Appl-null flies , because $Appl^{d}$ flies exhibit impaired electric shock avoidance [8, 20]; In such flies a defect in the aversive memory assay could result from an impairment in electric shock perception during conditioning and therefore not represent true memory defects. We showed here that $Appl^{d}$ also affects *vnd* function (Fig 2) and hence wondered if this impairment in electric shock avoidance was really due to the lack of the *Appl* function itself. In order to test this hypothesis, we evaluated the long-term memory (LTM) performance of $Appl^{C2.1}$/Y flies which are null for *Appl* but wild-type for *vnd*. The electric shock avoidance and olfactory acuity appears wild-type in $Appl^{C2.1}$ flies (Fig 6). Interestingly, $Appl^{C2.1}$ flies showed a complete loss of LTM, and this memory defect was fully rescued by the restricted expression of an *UAS-Appl* transgene in adult MBs (Fig 6). No rescue was detected in the non-induced 18°C

controls (S6 Fig). These results conclusively demonstrate that the specific and complete loss of Appl affects long-term memory independently from any potential defects during brain development.

Discussion

It has been proposed that Appl is part of the membrane complex formed by the core PCP proteins Fz and Vang [4]. *Appl*^{d} was, previous to this report, the only *Appl* null allele described. *Appl*^{d} mutant flies are completely lacking Appl function and exhibit 14.5 % MB β-lobe loss [15] in accordance with what has been reported [4, 5]. This modestly-penetrant axonal phenotype due to the lack of Appl could be due to partially redundant function provided by the other transmembrane receptors of the complex. In particular, flies homozygous for the loss of function allele *Vang*$^{stbm-6}$ exhibit 50% β-lobe loss [5]. As the *Appl*^{d} allele involves complex chromosomic rearrangements [8], we decided to leverage CRISPR in order to produce a definitive deletion of around 50 kb to specifically eliminate the *Appl* transcriptional unit. We recovered two *Appl* complete deletions: *Appl*$^{C1.4}$ and *Appl*$^{C2.1}$ removing around 52 kb and 48 kb and exhibiting 66 % and 9 % β-lobe loss respectively. DNA sequences analysis revealed that, while the *Appl*$^{C2.1}$ deletion removes only *Appl* sequences, the *Appl*$^{C1.4}$ deletion additionally removes a part of the proximally located transcriptional unit corresponding to the *vnd* gene (Fig 1). This indicates that in addition to Appl, *vnd* is likely involved in the β-branch axon outgrowth. Moreover, as can be expected from the extent of the deletions and based on genetic complementation tests, *Appl*$^{C1.4}$ deletion, but not *Appl*$^{C2.1}$ deletion, affects *vnd* function. Most importantly, the *Appl*^{d} deletion, which removes most of the Appl coding sequence and also the intergenic region between *Appl* and *vnd*, also affects *vnd* function (Fig 1 and 2). The role of *vnd* in β-branch axon outgrowth is complicated by the fact that the *vnd* viable mutant alleles (*Appl*^{d} *and Appl*$^{C1.4}$ deletions), are associated with the lack of *Appl* function. Nevertheless, employing a small (less than 100 kb) genomic *Appl*$^{+}$ duplication, we found that flies lacking only *vnd* function exhibit 69% β-lobe loss that is completely rescued by a small genomic *vnd*$^{+}$ duplication (Fig 4). This demonstrates the requirement of *vnd* function for MB β-branch axon outgrowth. To better understand the roles of both Vnd isoforms in the MB β-branch axon outgrowth, we produced two mutations, *vnd*$^{C\Delta B}$ and *vnd*$^{C\Delta A}$, which remove the *vnd-B* and the *vnd-A* transcript respectively (Fig 3 and S3 Fig). Surprisingly, although Vnd-A has a significant role in MB axon growth, apparently Vnd-B plays little to no role in this process. Noticeably, MB phenotype of *Appl*$^{C1.4}$/*vnd*$^{C\Delta A}$ flies is similar in penetrance to the one of *Appl*$^{C1.4}$/*vnd*^{A}, indicating that the lack of *vnd-A* function seems to have the same effect than the complete lack of both *vnd* functions.

It may have been anticipated that Vnd, a transcription factor, was required within the MBs and was probably being part of the Appl signaling pathway in order to act on axon growth. Consequently, Vnd should have been expressed within the MBs and the *vnd* function was expected to be cell-autonomous. However, endogenous *vnd* transcription monitored by GAL4 expression that is translated from the same mRNA transcript and validated by an anti-Vnd antibody show no sign of expression within the MBs. Rather, *vnd* is transcribed within a neuronal brain structure in close proximity to the developing MB medial lobe from which the adult β lobe develops (Fig 5). Also, using MARCM mosaic analysis, we show that β axons extended from MB clones null for *vnd* function exhibit wild-type growth patterns (S5 Fig) demonstrating a non-cell-

autonomous requirement for Vnd. Therefore, we favor the hypothesis where *vnd* expressed in a MB surrounding brain structure is generating, directly or indirectly, one or several secreted factors that will act on the axon growth of the developing β medial lobe.

Prior to this study, it was not possible to evaluate the effects of a complete lack of *Appl* in aversive olfactory memory due to the failure of $Appl^{d}$ mutants to show normal shock reactivity [8, 20]. It was therefore hypothesized that it was the lack of Appl *per se* which was the cause of this impairment in electric shock avoidance. We reevaluated this hypothesis with the $Appl^{C2.1}$ allele which removes only the *Appl* function. Flies bearing only a deletion of *Appl* react normally to electric shock and olfactory cues similarly to control flies but show a total lack of 24h memory after a long-term conditioning (Fig 6). Therefore, it is not the lack of *Appl* function in the $Appl^{d}$ mutants which is the origin of the impairment in electric shock avoidance. Importantly, the memory defect can be completely rescued by the expression of $Appl^{+}$ solely in the post-development adult MBs. This demonstrates that a complete lack of *Appl* results in a specific memory defect independently of any role that Appl might have in the developing brain. Consequently, the modest mutant MB axonal growth morphological phenotype displayed by the $Appl^{C2.1}$ allele likely has no measurable impact on long-term memory. This is in accordance with the requirement of the vertical lobes but not the median lobes in aversive long-term memory [21].

The accumulation of amyloid-β (Aβ) is a hallmark feature of AD [22, 23]. Nevertheless, the production of Aβ peptides is at the expense of the full-length APP protein levels, whose roles in AD are, as yet, unclear. The *Drosophila* memory defect due to the complete lack of *Appl* may therefore be relevant to the memory defects associated with human AD. Therefore, our observation that the memory defect resulting from the complete lack of *Appl* could be completely rescued by the expression of $Appl^{+}$ in a specific adult brain region, thus bypassing any potential role of APPL in development could be of significance to our understanding of the molecular basis of AD.

Materials and methods

Drosophila stocks

All crosses were performed on standard culture medium at 25° C. Except where otherwise stated, all alleles and transgenes have been described previously (http://flystocks.bio.indiana.edu/). The following alleles were used: $Appl^{C1.4}$, $Appl^{C2.1}$, $vnd^{C\Delta A}$ and $vnd^{C\Delta B}$ were generated in this study. *Appl-y*$^{+}$ (BL #56073), $Appl^{d}$ (BL #43632), $Vang^{stbm-6}$ (BL #6918) and vnd^{A} (BL #57139), $vnd^{\Delta 38}$ [24](Chu 1998), vnd^{6} [12](Jimenez 1995). The following transgenes were used: *UAS-mCD8::GFP* (BL #5137), *UAS-Appl* (BL #38403) and the duplications resulting from genomic transgenes *Dp-Appl*$^{+}$ (BL #32288) and *Dp-vnd*$^{+}$ (BL #30219) both inserted into the same attP site at 65B2. We used three GAL4 lines: *vnd-T2A-GAL4* which reveals *vnd* transcription, *c739-GAL4* (BL #7362) expressed in adult αβ MB neurons [25] and VT30559 expressed in adult MB neurons [26]. Recombinant chromosomes were obtained by standard genetic procedures and were molecularly verified.

CRISPR-Cas9 strategy

All guide RNA sequences (single guide RNA (sgRNA)) were selected using the algorithm targetfinder.flycrispr.neuro.brown.edu/ containing 20 nucleotides each (PAM excluded) and are

predicted to have zero off-targets. We selected one pair of sgRNA for the *Appl* gene and two pairs of sgRNA for the *vnd* gene. For *Appl*, the pair is targeting the all transcriptional unit (S2 Fig). For *vnd*, each pair is targeting either the A specific region of *vnd* or the B specific region of *vnd* (S3 Fig). We used the following oligonucleotide pairs: CRISPR-1 Appl fwd and CRISPR-1 Appl rev to target the all *Appl* region, CRISPR-1 vnd A fwd and CRISPR-1 vnd A rev to target the A region of *vnd*, CRISPR-1 vnd B fwd and CRISPR-1 vnd B rev to target the B region of *vnd* (see the corresponding oligonucleotide sequences in S2 and S3 Fig.). We introduced two sgRNA sequences into pCFD4 [14], a gift from Simon Bullock (Addgene plasmid # 49411) by Gibson Assembly (New England Biolabs) following the detailed protocol at crisprflydesign.org. For PCR amplification, we used the protocol described on that website. Construct injection was performed by Bestgene (Chino Hills, CA) and all the transgenes were inserted into the same attP site (VK00027 at 89E11). Being aware that the DNA excision of nearly 50 kb might be rare, we have decided to use a positive screen before validation by genomic PCR. We have used a stock where the *Appl* gene is marked by a y^+ construct. The deletion of the *Appl* gene should therefore be associated to y^- phenotype. Transgenic males expressing the *Appl* sgRNAs and bearing an isogenized X chromosome (*y Appl-y^+ Act-Cas9 w**) were crossed to *FM7c/ph^0 w* females. 180 crosses were set up and only two crosses gave rise to *y Appl$^{deletion?}$ Act-Cas9 w*/FM7c* females indicating 1% of CRISPR efficacy. From each of these two crosses, a single *y Appl^{deletion} Act-Cas9 w* /FM7c* female was crossed with *FM7c* males to make a stock (*Appl$^{C1.4}$* and *Appl$^{C2.1}$* where Cas9 was removed). The deletion were then validated by genomic PCR using two couples of primers: *Appl$^{C1.4}$* fwd (GAGCCAGATACACAAGCACA) / *Appl$^{C1.4}$* rev (GGCTTTGTTTACTTCCTGGC) and *Appl$^{C2.1}$* fwd (TCCTACTACGTTCCACAATC) / *Appl$^{C2.1}$* rev (TAATGCCCAACATATCCAAC). The precise endpoints of the deletion were determined by sequencing (Genewiz, France). Transgenic males expressing the different *vnd* sgRNAs were crossed to *y nos-Cas9 w** females bearing an isogenized X chromosome. 100 crosses were set up for each sgRNA pair, with up to 5 males (because of poor viability) containing both the sgRNAs and *nos-Cas9,* and 5 *FM7c/ph^0 w* females. From each selected cross, a single *y vnd$^{deletion?}$ nos-Cas9 w* /FM7c* female was crossed with *FM7c* males to make a stock which was validated for the presence of an indel by genomic PCR with primers flanking the anticipated deletion and the precise endpoints of the deletion were determined by sequencing (Genewiz, France) using *vnd*-specific primers: *vnd$^{C\Delta A}$* fwd (ccaacaaagccgagagtctct) / *vnd$^{C\Delta A}$* rev (cgggaatttctaagccagggt) and *vnd$^{C\Delta B}$* fwd (cgatttggggcgttgtgagta) / *vnd$^{C\Delta B}$* rev (gttgggctttaatccgggagt). A CRISPR efficacy of at least 5% was obtained in both cases. We kept a single stock from each set of CRISPR experiment: *vnd$^{C\Delta A}$* and *vnd$^{C\Delta B}$* where Cas9 was removed.

Brain dissection, immunostaining and MARCM mosaic analysis

Adult fly heads and thoraxes were fixed for 1 h in 3.7% formaldehyde in phosphate-buffered saline (PBS) and brains were dissected in PBS. For larval and pupal brains, brains were first dissected in PBS and then fixed for 15 min in 3.7% formaldehyde in PBS. They were then treated for immunostaining as described [19, 27]. Antibodies, obtained from the Developmental Studies Hybridoma Bank, were used at the following dilutions: Mouse monoclonal anti–Fas2 (1D4) 1:10 , mouse monoclonal anti-Repo (8D1.2) 1:10 and guinea pig polyclonal anti-vnd (1/1000). Goat secondary antibodies conjugated to Cy3 against mouse or guinea pig IgG (Jackson Immunoresearch laboratory) were used at 1:300 for detection. DAPI (Sigma) was used after secondary antibody washes. Tissues were incubated 10 minutes at room temperature in a 1/1000

306 solution from a stock containing 1 mg/ml of DAPI solution, then washed. To generate clones in
307 the MB, we used the MARCM technique [19]. First instar larvae were heat-shocked at 37°C for 1
308 h. Adult brains were fixed for 15 min in 3,7% formaldehyde in PBS before dissection and GFP
309 visualization.
310
311 **Production of the anti-Vnd antiserum**
312 Full length vnd-RA was amplified via PCR from cDNA and cloned into a pRSET bacterial expression
313 vector (ThermoFisher) in frame with an N-terminal 6x-His tag, amplified in DH5alpha and
314 transformed into BL21 competent cells for protein production. His-tagged VndA was purified over
315 a Nickel-NTA agarose resin (Qiagen) according to manufacturer's recommendation. Purified
316 protein was injected into guinea pigs by Squarix GmbH (Marl, Germany, www.squarix.de),
317 selected by assuring that pre-bleeds did not produce signal in Western blots of fly extracts.
318 Successive bleeds were screened for distinct signal in Western blots using embryo extracts and
319 by immunohistochemistry, where signal was expected post 2.5hrs AED.
320
321 **Behavior experiments**
322 For behavior experiments, flies were raised on standard medium at 18°C and 60% humidity in a
323 12-h light/dark cycle. We used the TARGET system [28] to inducibly express UAS-*Appl*$^{+}$ construct
324 exclusively in adult flies and not during development. 0-3 day old flies were transferred to fresh
325 bottles containing standard medium and kept at 30.5°C for 2 days before conditioning. For non-
326 induced experiments, flies were transferred to fresh bottles containing standard medium and
327 kept at 18°C before conditioning. All the behavior experiments, including the sample sizes, were
328 conducted similarly to other studies [29]. Groups of 20-50 flies were subjected to olfactory
329 conditioning protocol consisting of five associative cycles spaced by 15min inter-trial intervals (5x
330 spaced training). Conditioning was performed at 25°C using previously described barrel-type
331 machines that allow the parallel training of up to 6 groups [21]. Throughout the conditioning
332 protocol, each barrel was plugged into a constant air flow at 2 L/min. For a single cycle of
333 associative training, flies were first exposed to an odorant (the CS+) for 1 min while 12 pulses of
334 5s long 60 V electric shocks were delivered; flies were then exposed 45 s later to a second odorant
335 without shocks (the CS-) for 1 min. The odorants 3-octanol (Fluka 74878, Sigma-Aldrich) and 4-
336 methylcyclohexanol (Fluka 66360, Sigma-Aldrich), diluted in paraffin oil to a final concentration
337 of 2.79·10-1 g/L, were alternately used as conditioned stimuli. During unpaired conditionings, the
338 odor and shock stimuli were delivered separately in time, with shocks occurring 3 min before the
339 first odorant. Flies were kept at 18°C on standard medium between conditioning and the memory
340 test. The memory test was performed at 25°C in a T-maze apparatus [30](Tully 1985), 24 h after
341 spaced training. Each arm of the T-maze was connected to a bottle containing 3-octanol and 4-
342 methylcyclohexanol, diluted in paraffin oil to a final concentration identical to the one used for
343 conditioning. Flies were given 1 min to choose between either arm of the T-maze. A performance
344 score was calculated as the number of flies avoiding the conditioned odor minus the number of
345 flies preferring the conditioned odor, divided by the total number of flies. A single performance
346 index value is the average of two scores obtained from two groups of genotypically identical flies
347 conditioned in two reciprocal experiments, using either odorant (3-octanol or 4-
348 methylcyclohexanol) as the CS^{+}. The indicated 'n' is the number of independent performance
349 index values for each genotype. The shock response tests were performed at 25°C by placing flies

in two connected compartments; electric shocks were provided in only one of the compartments. Flies were given 1 min to move freely in these compartments, after which they were trapped, collected, and counted. The compartment where the electric shocks were delivered was alternated between two consecutive groups. Shock avoidance was calculated as for the memory test. Because the delivery of electric shocks can modify olfactory acuity, our olfactory avoidance tests were performed at 25°C on flies that had first been presented another odor paired with electric shocks. Innate odor avoidance was measured in a T-maze similar to those used for memory tests, in which one arm of the T-maze was connected to a bottle with odor diluted in paraffin oil and the other arm was connected to a bottle with paraffin oil only. Naive flies were given the choice between the two arms during 1 min. The odor-interlaced side was alternated for successively tested groups. Odor concentrations used in this assay were the same as for the memory assays. At these concentrations, both odorants are innately repulsive.

Microscopy and image processing

Images were acquired at room temperature using a Zeiss LSM 780) equipped with a 40x PLAN apochromatic 1.3 oil-immersion differential interference contrast objective lens and a Leica SP8 laser scanning confocal microscopes (MRI Platform, Institute of Human Genetics, Montpellier, France. The immersion medium used was Immersol 518F. The acquisition software used was Zen 2011 (black edition) for the Zeiss and LasX for the Leica. Contrast and relative intensities of the green (GFP), of the red (Cy3) and of the DAPI channels were processed with ImageJ (Fiji) software. Settings were optimized for detection without saturating the signal.

Statistics

Comparison between two groups expressing a qualitative variable was analyzed for statistical significance using the Chi^2 test. (BiostaTGV: http://biostatgv.sentiweb.fr/?module=tests). For behavior experiments, all data are presented as mean ± SEM. 2 groups of about 30 flies were reciprocally conditioned, using respectively octanol or methylcyclohexanol as the CS^+. The memory score was calculated from the performance of two groups as described above, which represents a single experimental replicate. Comparisons of the data series between two conditions were achieved by a two-tailed unpaired t-test. Comparisons between more than two distinct groups were made using a one-way ANOVA test, followed by Tukey pairwise comparisons between the experimental groups and their controls. ANOVA results are presented as the value of the Fisher distribution F(x,y) obtained from the data, where x is the number of degrees of freedom between groups and y is the total number of degrees of freedom for the distribution. In the figures, asterisks illustrate the significance level of the t-test, or of the least significant pairwise comparison following an ANOVA. Values of $p < 0.05$ were considered to be significant. Statistical significance was defined as: ns = not statistically different, **p<0.01 and****p<0.0001.

Figure legends

Fig 1. Generating new *Appl* CRISPR alleles.

(A) Schematic representation of *Appl* (blue) and *vnd* (green) genes and transcripts. White boxes represent 5'UTR and 3'UTR, blue and green boxes represent *Appl* and *vnd* coding sequences

respectively. Schematic representations of the $Appl^{d}$, $Appl^{C1.4}$ and $Appl^{C2.1}$ mutant alleles where the deleted sequences are represented in light blue. The hatched black segment represents the uncertainty where the deletion of $Appl^{d}$ starts in 5'. (B) Representation of the 3' limit of the $Appl^{d}$, $Appl^{C1.4}$ and $Appl^{C2.1}$ mutant alleles (light blue). The hatched black segment represents the uncertainty where the $Appl^{d}$ deletion ends in 3'. The orange star represents the position of the 3' sgRNA used to create the two CRISPR deletions. (C) Wild-type (WT) MB revealed by an anti-Fas2 staining. The pink and yellow arrowheads show respectively the α and β lobe (n=216 MBs). (D-E) Anti-Fas2 staining reveals the loss of β lobe on a representative $Appl^{C1.4}$ brain (n=147 MBs) (D) and on $Appl^{C2.1}$ brain (n=253 MBs) (E). The % represents the proportion of loss of β lobe for each genotype. Scale bar = 50 µm.

Fig 2. $Appl^{d}$ and $Appl^{C1.4}$, but not $Appl^{C2.1}$, are impaired for *vnd* function.
A) Schematic representation of *vnd* gene and transcripts. White boxes represent 5'UTR and 3'UTR, green boxes represent coding sequences. Red star represents point mutation on vnd^{A} allele. Schematic representation of *vnd-B* and *vnd-A* transcripts. The vnd^{A} mutation affects both transcripts. (B-D) Anti-Fas2 staining reveals the loss of β lobe on a representative $Appl^{d}$/ vnd^{A} brain (n=214 MBs) (B), $Appl^{C1.4}$/ vnd^{A} brain (n=147 MB) (C) but not on $Appl^{C2.1}$/ vnd^{A} brain (n=248 MBs) (D). The % represents the proportion of loss of β lobe for each genotype. Scale bar = 50 µm.

Fig 3. Generating new *vnd* CRISPR alleles deleted either for the *vnd-B* or the *vnd-A* function.
(A) Schematic representation of *vnd* gene and transcripts. White boxes represent 5'UTR and 3'UTR, green boxes represent coding sequences. The hatched black boxes represent the deleted region of $vnd^{C\Delta A}$ and $vnd^{C\Delta B}$ (B-C) Anti- Fas2 staining reveals essentially wild-type looking MBs on a representative $vnd^{C\Delta B}$ brain (n=146 MBs) (B) and $Appl^{C1.4}$/ $vnd^{C\Delta B}$ brain (n=159 MB) (C). The % represents the proportion of loss of β lobe for each genotype. Scale bar = 50 µm.

Fig 4. Vnd-A is required for MB β-branch axon outgrowth.
(A) Quantitation of the rescue of MB β lobe absence of $Appl^{C1.4}$/Y (66%; n= 147 MBs, see a representative brain in Fig.1D) and $Appl^{C1.4}$/$vnd^{C\Delta A}$ (64%; n=198 MBs) (light blue) by an *Appl* duplication (dark blue) (50%; n=150 MBs, 69%; n=89 MBs) and by a *vnd* duplication (green) (3%; n=191 MBs ; 0%; n=164 MBs). **p<0.01 and ****p<0.0001. (B-D) Anti-Fas2 staining on a representative rescued $Appl^{C1.4}$/Y; *Dp-vnd*$^{+}$/+ brain (B), $Appl^{C1.4}$/$vnd^{C\Delta A}$; +/+ brain (C) and on $Appl^{C1.4}$/$vnd^{C\Delta A}$; *Dp-vnd*$^{+}$/+ brain (D). The % represents the proportion of loss of β lobe for each genotype. Scale bar = 50 µm.

Fig 5. *vnd* is expressed close to the developing MB medial lobe.
(A-D) Visualization of *vnd* expression in brain using *vnd-GAL4* driven *UAS-GFP* at L3, 0h, 6h, and 24h APF. GFP was visualized on green and anti-FasII staining labelling of MB axons on red. A-D are confocal z stacks taken the whole MB and A'-D' are stacks of five plans from A-D respectively comprising GFP^{+} regions surrounding MB. Arrowheads point to *vnd-GAL4* driven *UAS-GFP* filamentous structures that surround MB medial lobes, which correspond to γ lobes from L3 to 6 h APF (A'-C') and β lobes at 24 h APF (D'). n $\geq$ 10 for each time point. (E-G) show single confocal plans showing *vnd* expression using *vnd-GAL4* driven *UAS-GFP* (single channel) at L3. E' to G' are merges of single channel E to G respectively and DAPI staining (red on E'), anti-vnd (red on F') and

anti-Repo (red on G'). DAPI labelled nuclei in honeycomb GFP$^+$ structures are pointed by arrows in E'. These nuclei were also vnd$^+$ (arrows in F') and they were not labelled by an anti-repo (white arrow in G') which labels glia nuclei (red dots pointed by a yellow arrow in G'). Scale bars are 50 μm. n $\geq$ 5 brains for each type of staining.

Fig 6. The long-term memory defect of *Appl*$^{C2.1}$/Y flies is rescued by *Appl*$^+$ expression in the adult mushroom body.

(A) Olfactory acuity was normal in *Appl*$^{C2.1}$/Y flies. For octanol**,** data presented as mean ± SEM. *t*-test n=12, t_{22} = 1.12, *P* = 0.26, ns: not significant. For methylcyclohexanol, data presented as mean ± SEM. *t*-test n=12, t_{22} = 1.51, *P* = 0.15, ns: not significant. (B) Shock reactivity was normal in *Appl*$^{C2.1}$/Y flies**.** Data presented as mean ± SEM. *t*-test. n=12, t_{22} = 1.47, *P* = 0.16, ns: not significant. (C) Flies only null for *Appl* have no measurable LTM which is fully rescued by the restricted expression of *Appl* in adult MBs. Data presented as mean ± SEM. n = 22-23, $F_{(4, 108)}$ = 16,41, *P* < 0.0001. Significance level of *t*-test or least significant pairwise comparison following ANOVA: ****p < 0.0001, ns: not significant.

Supporting information

S1 Fig. Scheme of *Appl*^{d} chromosomic organization

(A) Schematic representation of *Appl*^{d} mutant allele. The upper panel represents the wild-type (WT) X (black) and Y (orange) chromosomes. The *elav*, *Appl* and *vnd* genes are represented respectively in yellow, blue, and green boxes. The middle panel represents the deficiency Df (1)RT518 on the X chromosome deleting the distal part of the chromosome including the *elav* and *Appl* genes. The X Dup Y chromosome represents a duplication of the X chromosome linked to the Y chromosome including the distal part of the X chromosome including the *elav* gene. The lower panel represents a proposed structure of the *Appl*^{d} chromosome where the deficiency bearing X chromosome had been linked by gamma rays to the X Dup Y chromosome (adapted from [8]).

S2 Fig. Structure of the *Appl*$^{C1.4}$ and *Appl*$^{C2.1}$ CRISPR alleles

(A) Schematic representation of *Appl* (blue) and *vnd* (green) genes and transcripts. White boxes represent 5'UTR and 3'UTR, blue and green boxes represent *Appl* and *vnd* coding sequences respectively. The yellow stars in *Appl* 5' region and the orange star in *Appl* 3' region represent the position of the sgRNA used to create *Appl*$^{C1.4}$ and *Appl*$^{C2.1}$ mutants. The red and blue boxes represent respectively the regions magnified in B and C. (B) Representation of the 5' sequence targeted by the sgRNA (yellow) and the PAM domain (magenta) in the WT chromosome *Appl* (blue) (upper line). The lower line is the sequence of the *Appl*$^{C1.4}$ mutant showing the beginning of the deletion about 1kb after the region targeted by the sgRNA. (C) Representation of the 3' sequence targeted by the sgRNA (orange) and the PAM domain (magenta) in the WT chromosome *Appl* (blue) and *vnd* (green) (upper line). The lower line is the sequence of the *Appl*$^{C1.4}$ mutant showing the end of the deletion about 6kb after the region targeted by the sgRNA. (D) Representation of the 5' and 3' sequences targeted by the sgRNA (yellow in 5' and orange in 3') and the PAM domain (magenta) in the WT chromosome *Appl* (blue) (upper line). The lower line

is the sequence of the *Appl*$^{C2.1}$ mutant showing the beginning of the deletion in the sequence targeted by the 5' sgRNA (yellow) and the end of the deletion in the sequence targeted by the 3' sgRNA (orange).

S3 Fig. Structure of the *vnd*$^{C\Delta B}$ and *vnd*$^{C\Delta A}$ CRISPR alleles

(A) Schematic representation of *vnd* (green) gene and transcripts. White boxes represent 5'UTR and 3'UTR, green boxes represent *vnd* coding sequences. The yellow stars represent the position of the sgRNA used to create *vnd*$^{C\Delta B}$ mutant. The orange stars represent the position of the sgRNA used to create *vnd*$^{C\Delta A}$ mutant. (B) Representation of the sequences targeted by the sgRNA (yellow) and the PAM domain (blue) in the WT chromosome *vnd* (green) (upper line). The lower line is the sequence of the *vnd*$^{C\Delta B}$ mutant showing the beginning of the deletion in the sequence targeted by the 5' sgRNA (yellow) and the end of the deletion in the sequence targeted by the 3' sgRNA (yellow). (C) Representation of the sequences targeted by the sgRNA (orange) and the PAM domain (blue) in the WT chromosome *vnd* (green) (upper line). The lower line is the sequence of the *vnd*$^{C\Delta A}$ mutant showing the beginning of the deletion at one nucleotide from the sequence targeted by the 5' sgRNA (orange) and the end of the deletion withinin the sequence targeted by the 3' sgRNA (orange).

S4 Fig. Vnd L3 CNS labelling

(A-C) Visualization of *vnd* expression in VNC using both *vnd-GAL4* driven *UAS-GFP* (green) and an anti-vnd antibody (red) at L3 stages. Images A-C and A'-C' are the same confocal z-projection. Laser intensities leading to the green color were increased from B, C to B', C' in order to illustrate the perfect colocalization between the two markers. Low laser intensity allowed us to show red nuclear vnd staining in only some GFP$^+$ cell bodies (white arrowheads in A- C). Soma containing vnd$^+$ positive nuclei that do not seem to be surrounded by GFP in A-C, can be visualized by increased green laser intensity A'- C' (yellow arrowheads), which saturates somas visualized in A-C. Scale bars are 50 μm. n $\geq$ 5 brains.

S5 Fig. *vnd* null mutant clones

(A-B) A representative neuroblast MARCM clone in a wild-type (WT) brain (A) and in a *vnd*^{A} brain (B). Scale bar = 50 μm. (C) Number of clones obtained in WT , *vnd*^{A} , *vnd*^{6} and *vnd*$^{\Delta 38}$. Full genotypes: (A) *w* tubP-GAL80 hsFLP122 FRT19A/w*^{1118} *sn FRT19A; c739-GAL4 UAS-mCD8-GFP/+* (also control hsFLP122 in C). (B) *w* tubP-GAL80 hsFLP122 FRT19A/y vnd*^{A} *w FRT19A; c739-GAL4 UAS-mCD8-GFP/+* (also vnd^{A} in C). (C) control hsFLP1: *w tubP-GAL80 hsFLP1 FRT19A* (from the Bloomington stock 5133)/*w UAS-mCD8-GFP sn FRT19A*; *c739-GAL4 UAS-mCD8-GFP/+*. vnd^{6}: *w tubP-GAL80 hsFLP1 FRT19A/y vnd*^{6} *w UAS-mCD8-GFP sn FRT19A*; *c739-GAL4 UAS-mCD8-GFP/+*. vnd$^{\Delta 38}$: *w tubP-GAL80 hsFLP1 FRT19A/vnd*$^{\Delta 38}$ *w UAS-mCD8-GFP FRT19A*; *c739-GAL4 UAS-mCD8-GFP/+*.

S6 Fig. In absence of *Appl*$^+$ induction, *Appl*$^{C2.1}$/Y flies display a long-term memory defect. Data presented as mean ± SEM. n = 15, $F_{(4, 70)} = 17.62$, $P < 0.0001$. Significance level of *t*-test or least significant pairwise comparison following ANOVA: ****p < 0.0001.

Acknowledgments

We thank Aymeric Chartier (IGH, Montpellier) for fruitful discussions in order to obtain *Appl* CRISPR alleles and Natasha Danda and Nuran Demirbas for technical assistance. We thank the Bloomington *Drosophila* Stock Center (Indiana University), the BioCampus RAM-*Drosophila* facility and the BioCampus imaging facility MRI (Montpellier, France). We acknowledge BestGene and Genewiz for transgene service and DNA sequencing respectively. The 1D4 anti-Fasciclin II hybridoma and the 8D12 anti-Repo monoclonal antibody developed by Corey Goodman were obtained from the Developmental Studies Hybridoma Bank, created by the NICHD of the NIH and maintained at the University of Iowa, Department of Biology, Iowa City, IA 52242. We thank Chris Doe for the $vnd^{\Delta 38}$ and vnd^{6} alleles and Tzumin Lee for the *vnd-T2A-GAL4* line.

Funding: C.M. was supported by a PhD grant from the Ministère de l'Enseignement Supérieur et de la Recherche. C.M. and G.U.B. were supported by the Fondation pour la Recherche Médicale (FRM) respectively for the 4th PhD year and for a 3 year post-doctoral fellowship. Work in the laboratory of J.-M.D. was supported by the Centre National de la Recherche Scientifique (CNRS), the Association pour la Recherche sur le Cancer (grants PJA 20151203422), the FRM (Programme "EQUIPES FRM2016" project DEQ20160334870) and the ANR 2021 ORIO. Work in the laboratory of T.P. was supported by the Fonds ESPCI and the Fondation Langlois.

References

1. Soldano A, Hassan BA. Beyond pathology: APP, brain development and Alzheimer's disease. Curr Opin Neurobiol. 2014;27:61-7. Epub 2014/03/19. doi: 10.1016/j.conb.2014.02.003. PubMed PMID: 24632309.
2. Nicolas M, Hassan BA. Amyloid precursor protein and neural development. Development. 2014;141(13):2543-8. Epub 2014/06/26. doi: 10.1242/dev.108712. PubMed PMID: 24961795.
3. Selkoe DJ, Hardy J. The amyloid hypothesis of Alzheimer's disease at 25 years. EMBO Mol Med. 2016;8(6):595-608. Epub 20160601. doi: 10.15252/emmm.201606210. PubMed PMID: 27025652; PubMed Central PMCID: PMCPMC4888851.
4. Soldano A, Okray Z, Janovska P, Tmejova K, Reynaud E, Claeys A, et al. The Drosophila Homologue of the Amyloid Precursor Protein Is a Conserved Modulator of Wnt PCP Signaling. PLoS biology. 2013;11(5):e1001562. Epub 2013/05/22. doi: 10.1371/journal.pbio.1001562. PubMed PMID: 23690751; PubMed Central PMCID: PMC3653798.
5. Liu T, Zhang T, Nicolas M, Boussicault L, Rice H, Soldano A, et al. The amyloid precursor protein is a conserved Wnt receptor. Elife. 2021;10. Epub 20210909. doi: 10.7554/eLife.69199. PubMed PMID: 34515635; PubMed Central PMCID: PMCPMC8437438.
6. Lin S. The making of the Drosophila mushroom body. Front Physiol. 2023;14:1091248. Epub 20230113. doi: 10.3389/fphys.2023.1091248. PubMed PMID: 36711013; PubMed Central PMCID: PMCPMC9880076.
7. Lee T, Lee A, Luo L. Development of the Drosophila mushroom bodies: sequential generation of three distinct types of neurons from a neuroblast. Development. 1999;126(18):4065-76. PubMed PMID: 10457015.

8. Luo L, Tully T, White K. Human amyloid precursor protein ameliorates behavioral deficit of flies deleted for Appl gene. Neuron. 1992;9(4):595-605. Epub 1992/10/01. PubMed PMID: 1389179.

9. Cassar M, Kretzschmar D. Analysis of Amyloid Precursor Protein Function in Drosophila melanogaster. Front Mol Neurosci. 2016;9:61. Epub 2016/08/11. doi: 10.3389/fnmol.2016.00061. PubMed PMID: 27507933; PubMed Central PMCID: PMCPMC4960247.

10. Goguel V, Belair AL, Ayaz D, Lampin-Saint-Amaux A, Scaplehorn N, Hassan BA, et al. Drosophila amyloid precursor protein-like is required for long-term memory. J Neurosci. 2011;31(3):1032-7. Epub 2011/01/21. doi: 31/3/1032 [pii]
10.1523/JNEUROSCI.2896-10.2011. PubMed PMID: 21248128.

11. Stepchenko AG, Pankratova EV, Doronin SA, Gulag PV, Georgieva SG. The alternative protein isoform NK2B, encoded by the vnd/NK-2 proneural gene, directly activates transcription and is expressed following the start of cells differentiation. Nucleic Acids Res. 2011;39(13):5401-11. Epub 20110321. doi: 10.1093/nar/gkr121. PubMed PMID: 21422076; PubMed Central PMCID: PMCPMC3141242.

12. Jimenez F, Martin-Morris LE, Velasco L, Chu H, Sierra J, Rosen DR, et al. vnd, a gene required for early neurogenesis of Drosophila, encodes a homeodomain protein. EMBO J. 1995;14(14):3487-95. doi: 10.1002/j.1460-2075.1995.tb07355.x. PubMed PMID: 7628450; PubMed Central PMCID: PMCPMC394416.

13. Doudna JA, Charpentier E. Genome editing. The new frontier of genome engineering with CRISPR-Cas9. Science. 2014;346(6213):1258096. doi: 10.1126/science.1258096. PubMed PMID: 25430774.

14. Port F, Chen HM, Lee T, Bullock SL. Optimized CRISPR/Cas tools for efficient germline and somatic genome engineering in Drosophila. Proc Natl Acad Sci U S A. 2014;111(29):E2967-76. Epub 2014/07/09. doi: 10.1073/pnas.1405500111. PubMed PMID: 25002478; PubMed Central PMCID: PMCPMC4115528.

15. Marquilly C, Busto GU, Leger BS, Boulanger A, Giniger E, Walker JA, et al. Htt is a repressor of Abl activity required for APP-induced axonal growth. PLoS Genet. 2021;17(1):e1009287. Epub 2021/01/20. doi: 10.1371/journal.pgen.1009287. PubMed PMID: 33465062; PubMed Central PMCID: PMCPMC7845969.

16. Haelterman NA, Jiang L, Li Y, Bayat V, Sandoval H, Ugur B, et al. Large-scale identification of chemically induced mutations in Drosophila melanogaster. Genome Res. 2014;24(10):1707-18. doi: 10.1101/gr.174615.114. PubMed PMID: 25258387; PubMed Central PMCID: PMCPMC4199363.

17. Lee YJ, Yang CP, Miyares RL, Huang YF, He Y, Ren Q, et al. Conservation and divergence of related neuronal lineages in the Drosophila central brain. Elife. 2020;9. Epub 20200407. doi: 10.7554/eLife.53518. PubMed PMID: 32255422; PubMed Central PMCID: PMCPMC7173964.

18. Chen HM, Huang Y, Pfeiffer BD, Yao X, Lee T. An enhanced gene targeting toolkit for Drosophila: Golic+. Genetics. 2015;199(3):683-94. Epub 20150102. doi: 10.1534/genetics.114.173716. PubMed PMID: 25555988; PubMed Central PMCID: PMCPMC4349064.

19. Lee T, Luo L. Mosaic analysis with a repressible cell marker for studies of gene function in neuronal morphogenesis. Neuron. 1999;22(3):451-61. PubMed PMID: 10197526.

20. Bourdet I, Preat T, Goguel V. The full-length form of the Drosophila amyloid precursor protein is involved in memory formation. J Neurosci. 2015;35(3):1043-51. doi: 10.1523/JNEUROSCI.2093-14.2015. PubMed PMID: 25609621; PubMed Central PMCID: PMCPMC6605540.
21. Pascual A, Preat T. Localization of long-term memory within the Drosophila mushroom body. Science. 2001;294(5544):1115-7. PubMed PMID: 11691997.
22. Palop JJ, Mucke L. Amyloid-beta-induced neuronal dysfunction in Alzheimer's disease: from synapses toward neural networks. Nat Neurosci. 2010;13(7):812-8. doi: 10.1038/nn.2583. PubMed PMID: 20581818; PubMed Central PMCID: PMCPMC3072750.
23. Musiek ES, Holtzman DM. Three dimensions of the amyloid hypothesis: time, space and 'wingmen'. Nat Neurosci. 2015;18(6):800-6. doi: 10.1038/nn.4018. PubMed PMID: 26007213; PubMed Central PMCID: PMCPMC4445458.
24. Chu H, Parras C, White K, Jimenez F. Formation and specification of ventral neuroblasts is controlled by vnd in Drosophila neurogenesis. Genes Dev. 1998;12(22):3613-24. doi: 10.1101/gad.12.22.3613. PubMed PMID: 9832512; PubMed Central PMCID: PMCPMC317241.
25. Aso Y, Grubel K, Busch S, Friedrich AB, Siwanowicz I, Tanimoto H. The mushroom body of adult Drosophila characterized by GAL4 drivers. J Neurogenet. 2009;23(1-2):156-72. Epub 2009/01/14. doi: 907683862 [pii]
10.1080/01677060802471718. PubMed PMID: 19140035.
26. Placais PY, de Tredern E, Scheunemann L, Trannoy S, Goguel V, Han KA, et al. Upregulated energy metabolism in the Drosophila mushroom body is the trigger for long-term memory. Nat Commun. 2017;8:15510. Epub 20170605. doi: 10.1038/ncomms15510. PubMed PMID: 28580949; PubMed Central PMCID: PMCPMC5465319.
27. Boulanger A, Clouet-Redt C, Farge M, Flandre A, Guignard T, Fernando C, et al. ftz-f1 and Hr39 opposing roles on EcR expression during Drosophila mushroom body neuron remodeling. Nat Neurosci. 2011;14(1):37-44. Epub 2010/12/07. doi: nn.2700 [pii]
10.1038/nn.2700. PubMed PMID: 21131955.
28. McGuire SE, Le PT, Osborn AJ, Matsumoto K, Davis RL. Spatiotemporal rescue of memory dysfunction in Drosophila. Science. 2003;302(5651):1765-8. PubMed PMID: 14657498.
29. de Tredern E, Rabah Y, Pasquer L, Minatchy J, Placais PY, Preat T. Glial glucose fuels the neuronal pentose phosphate pathway for long-term memory. Cell Rep. 2021;36(8):109620. doi: 10.1016/j.celrep.2021.109620. PubMed PMID: 34433052; PubMed Central PMCID: PMCPMC8411112.
30. Tully T, Quinn WG. Classical conditioning and retention in normal and mutant Drosophila melanogaster. J Comp Physiol [A]. 1985;157(2):263-77. PubMed PMID: 3939242.

Figure 1

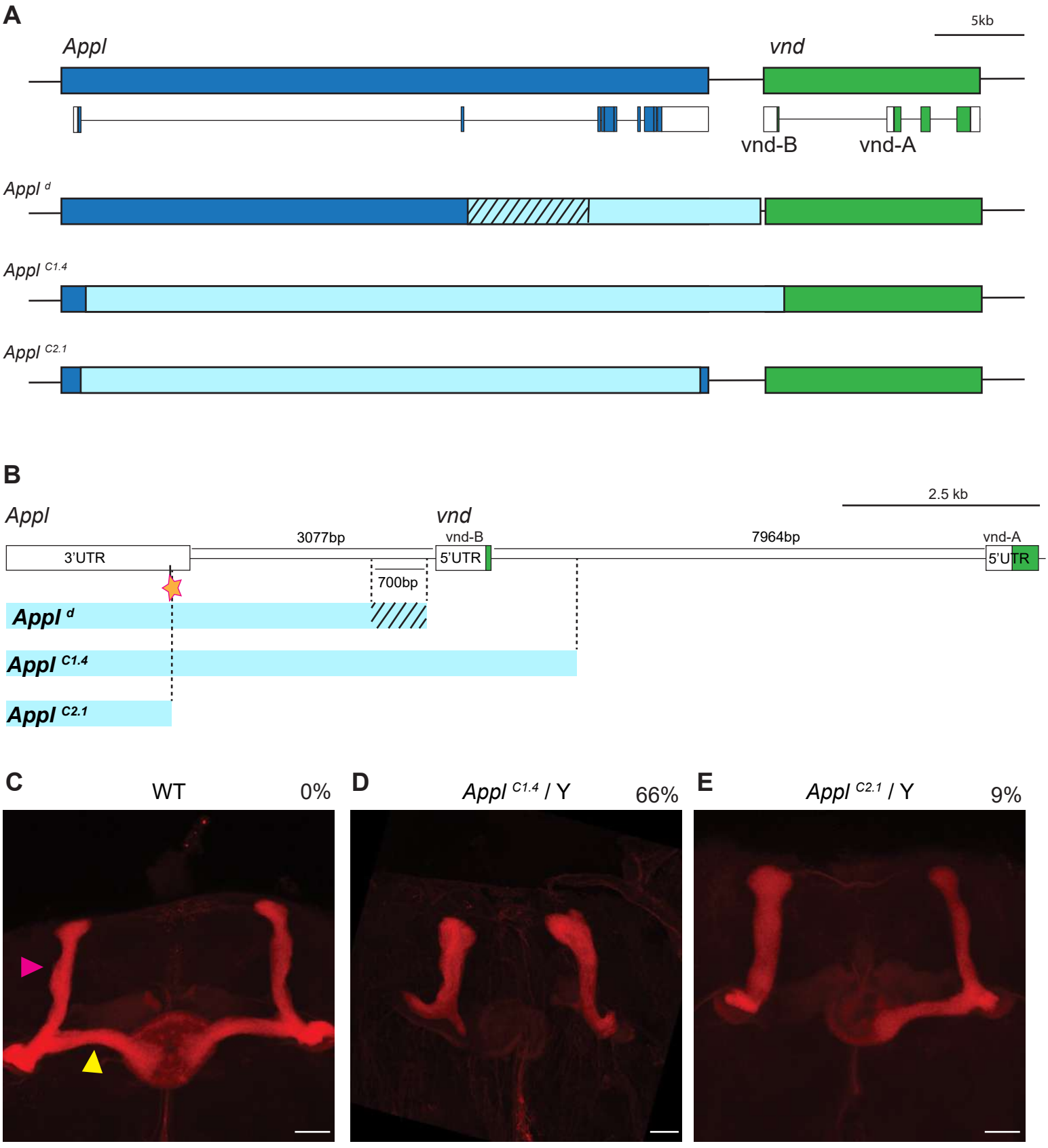

Figure 2

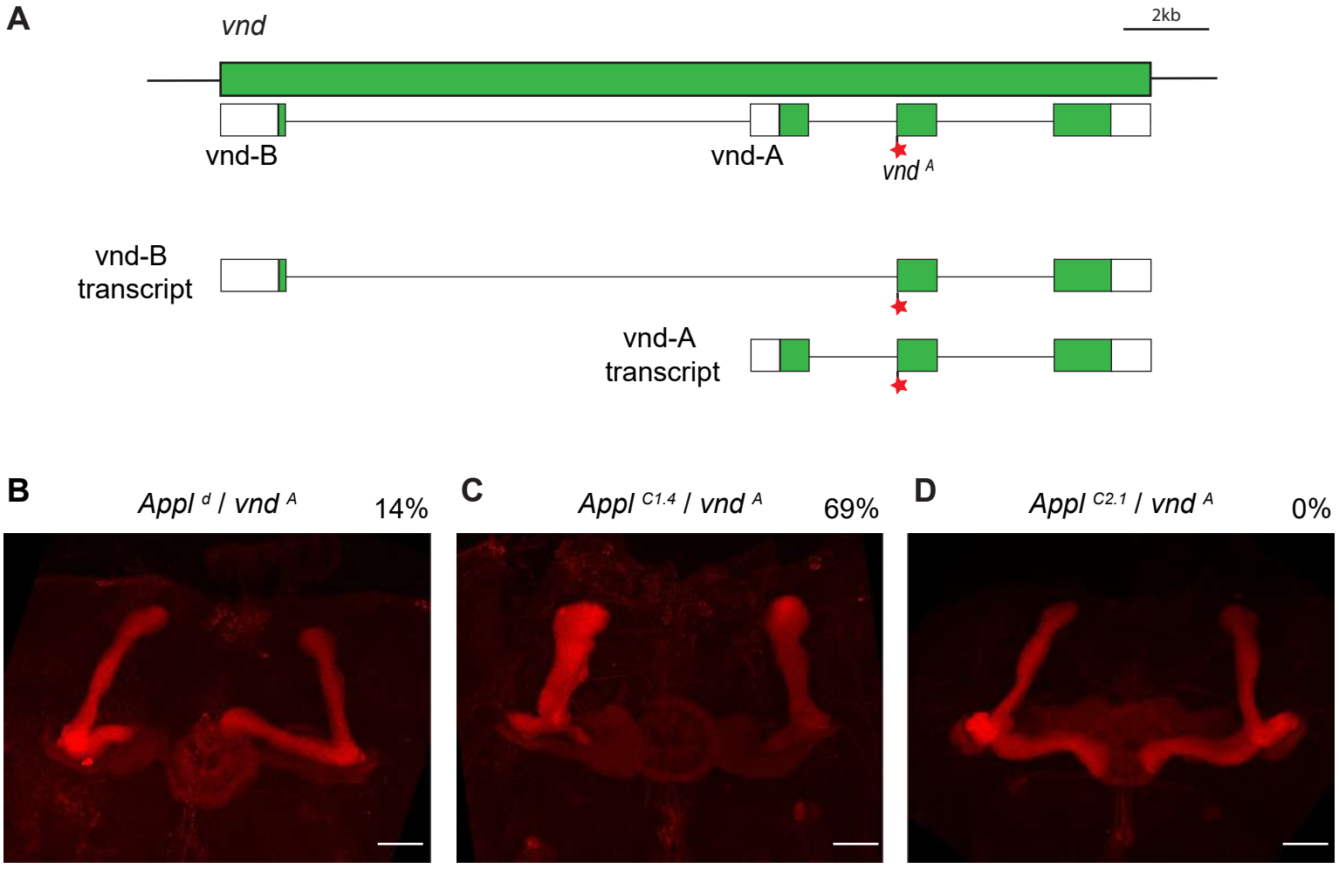

Figure 3

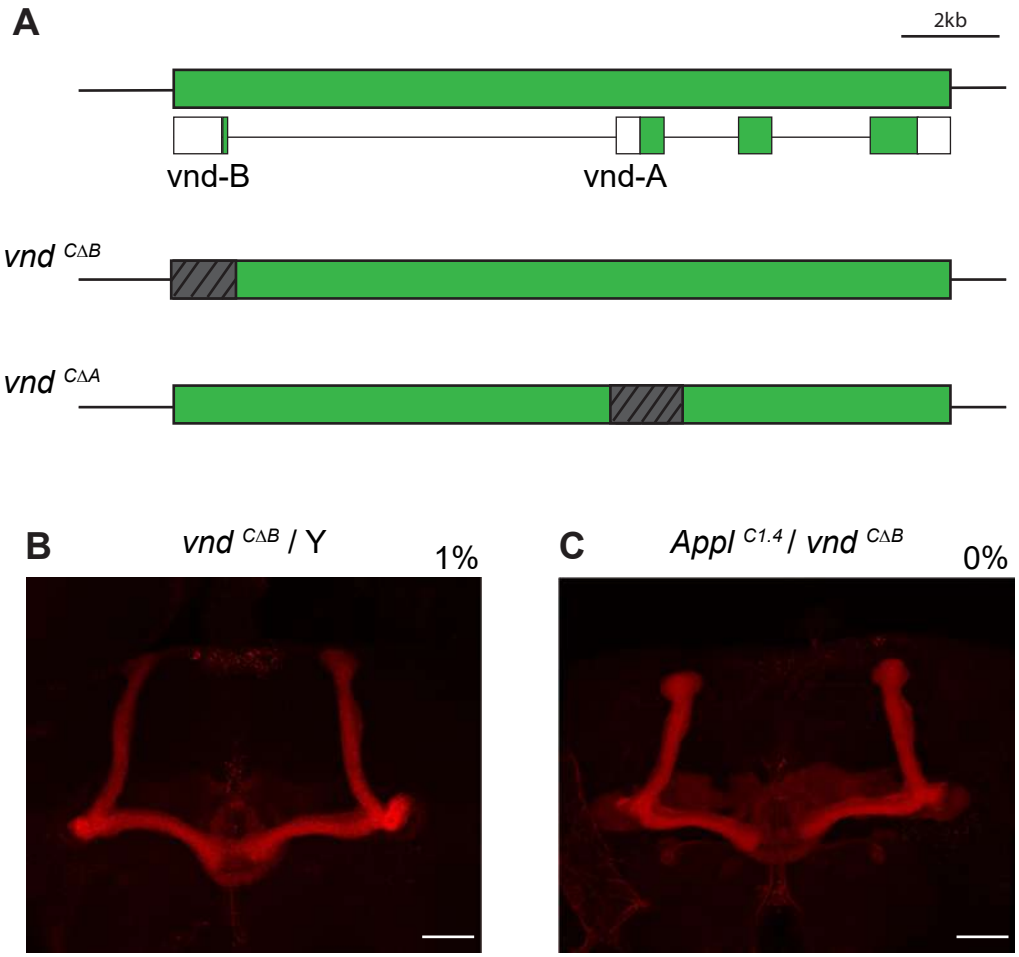

Figure 4

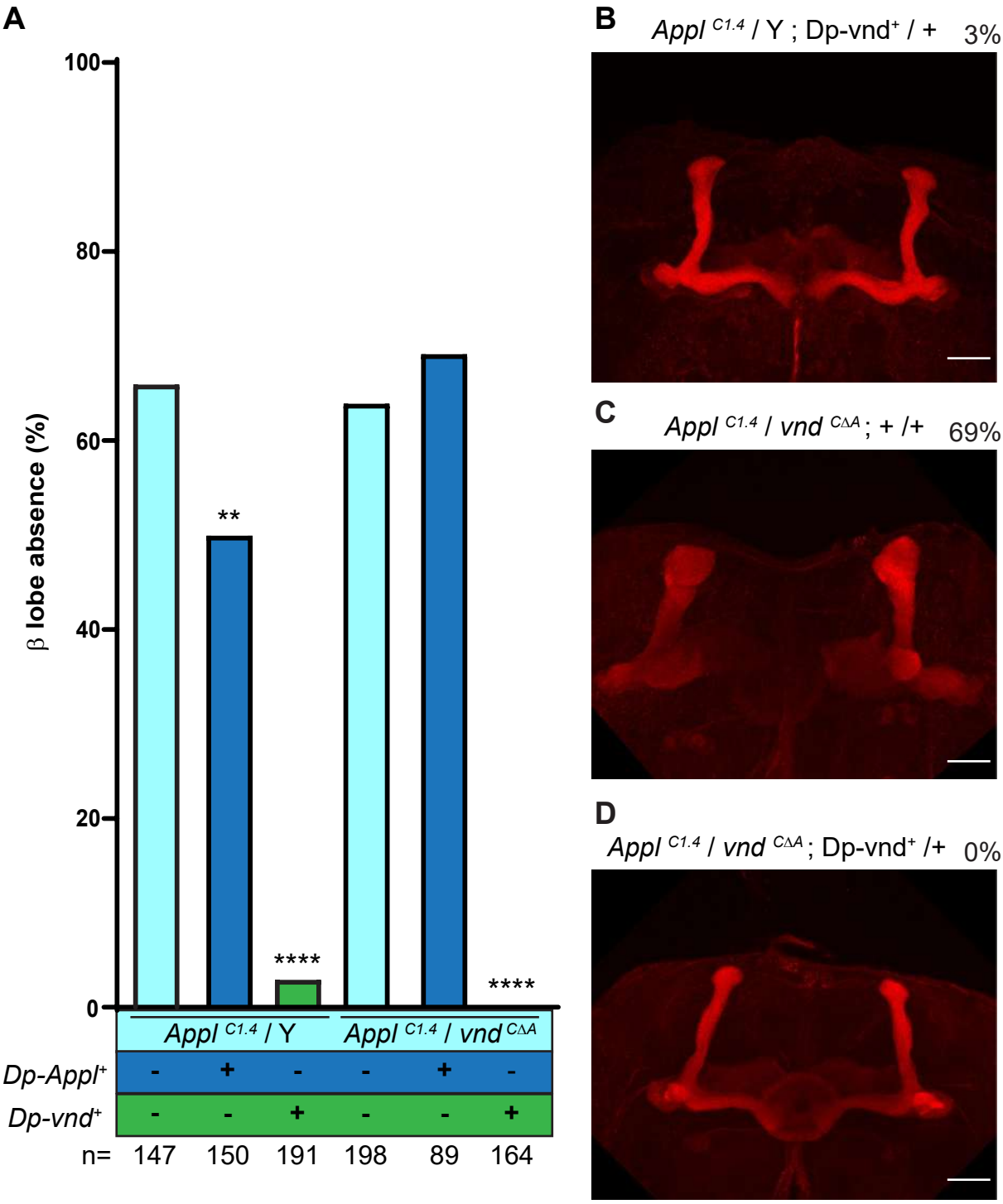

Figure 5

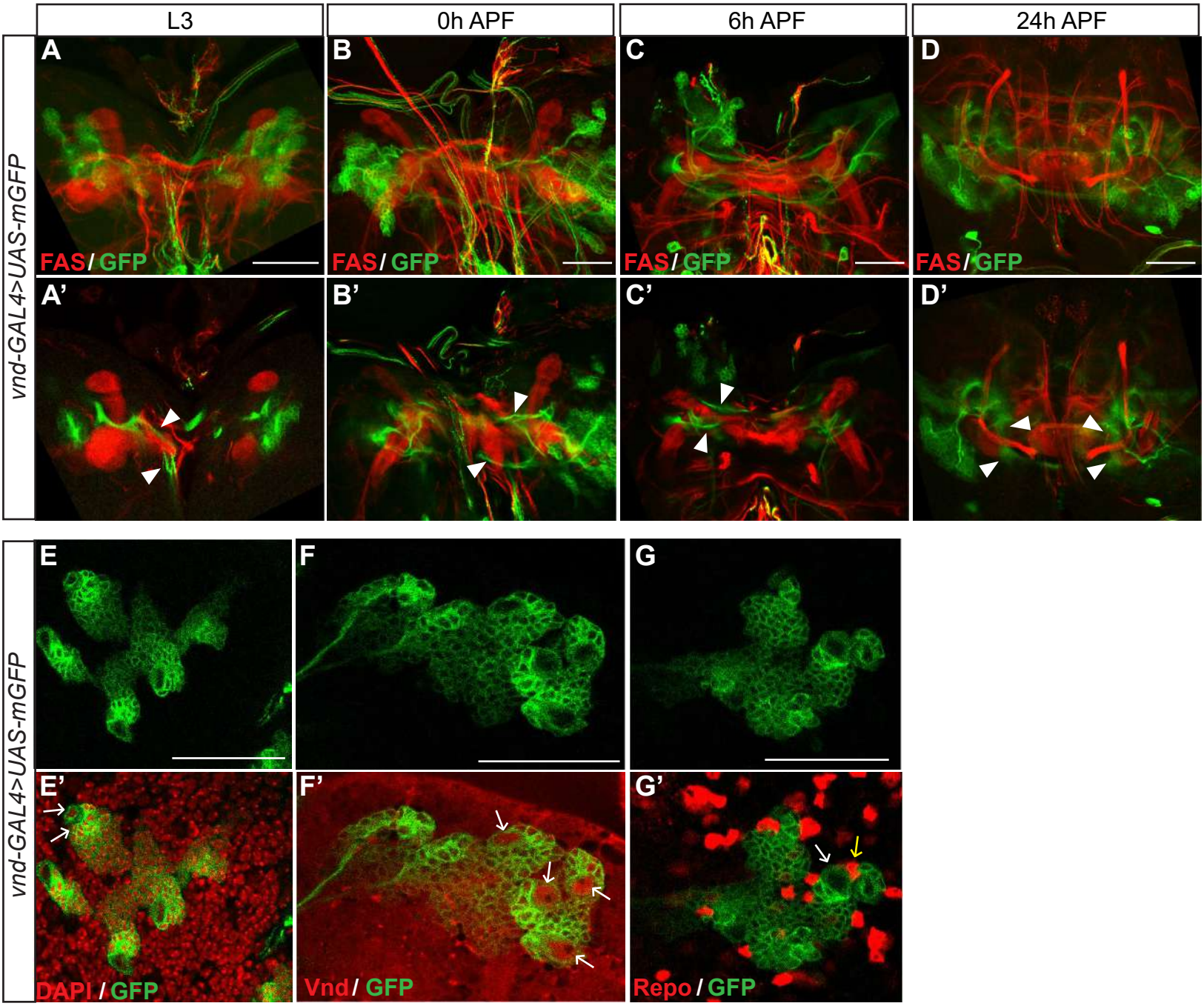

Figure 6